Assessment of the activation of collimators irradiated with clinical proton beams and development of a semi-empirical model for activity calculation

A. Carnicer[a], C. Candela-Juan[b], M. Nirrengarten[a], V. Blideanu[c], A. Mazal[b], J. Hérault[a], S. Delacroix[b]
[a]Centre Antoine Lacassagne (CAL), 227 avenue de la Lanterne, 06200 Nice, France
[b]Centre de Protonthérapie d'Orsay Institut Curie (ICPO), 15 Rue Georges Clemenceau, 91400 Orsay, France
[c]Commissariat à l'énergie atomique (CEA-Saclay), Bât. 135 Doseo, 91191 Gif-sur-Yvette, France

1. Introduction

Radiation therapy with proton beam presents outstanding advantages for some clinical targets over conventional radiotherapy thanks to the ballistic properties of protons, leading to excellent conformity of the dose distribution to the target tumor and sparing organs at risk, with no exit dose [1].

Passive and active beam delivery techniques are both used to conform the beam to the target volume [2]. In passive scattering, the proton beam is spread by placing one or two scatterers in the path of protons. The range and the spread out Bragg peak (SOBP) required in each treatment are obtained with a set of range shifters and range modulator wheels placed inside the nozzle. Passive scattering needs additional patient-specific beam-modifying devices to conform the dose to the treatment volume. At least a final collimator must be used to match the field aperture to the tumor contour. Many treatments require as well a compensator to match the distal shape to the tumor depth. In scanning-beam techniques the treatment volume is irradiated "voxel-by-voxel" by a narrow monoenergetic proton beam steered by magnets in successive layers of different depths, by adjusting the energy of the beam upstream of the nozzle. This active beam delivery technique generally avoids the use of beam-modifying devices, although range shifters and apertures might also be used for improved conformity.

Components placed in the path of the beam to modify the range (e.g. range shifter, compensators and filters) are typically made of a low-atomic number medium such as acrylic, equivalent to soft tissue density. Conversely, apertures or collimators are made of an alloy of high-atomic number elements, usually brass or bronze, thick enough to stop the proton beam. In a few cases, low melting points alloys are used (eg. Lipowitz alloy including bismuth, lead, tin and eventually cadmium). Tungsten is used for upstream collimators and a few number of multileaf collimators [3]. Nickel, iron and brass have been recommended to replace tungsten collimators related to their production of secondary neutrons, and their activation has been studied [4,5]. Combination of two elements, such as brass and stainless-steel [6], is also proposed in hybrid collimators to reduce treatment cost. Nuclear reactions produced by collisions of protons and secondary particles on fixed and removable components all along the beam line produce a range of isotopes in the irradiated materials from activation processes [7-9]. Activation depends on the particle type, target material, beam flux, beam energy distribution, and irradiation time profile. Unlike activation of acrylic materials, radioactive products induced in high-atomic number materials used in collimators, such as copper and zinc, are numerous and typically with longer half-lives.

As a result of activation, patient-specific devices represent a radiation safety matter with respect to both occupational exposure [10] and subsequent management and destination after use [11]. Patient collimators are particularly concerned by the second issue because of the longer half-lives of isotopes induced. The management modalities are subjected to local decrees imposed by national regulatory bodies as regards its radioactive content. To be properly applied, these rules require non trivial knowledge of the isotopes present in the pieces and their activities. Common detectors used in radiation safety are not appropriate because they typically measure total activities. Spectrometry is, to our best knowledge, the only experimental technique that allows both identification and quantification of isotopes. However, proton therapy centers do not necessarily have access to spectrometers with adequate resolution. An alternative to quantify individual isotope activities is Monte Carlo (MC) calculation, which turns out to be a particularly valuable tool to predict material activation provided the number and variability of parameters and the potential complexity of geometrical structures involved. Several MC codes such as FLUKA, MCNP, Geant4 and PHITS are used to this purpose. Among those, the FLUKA code has been widely benchmarked [12-14] and employed [3,8,15-25] for activation calculations and stands out for its suitability in this type of calculations [17]. FLUKA is based on models of high energy hadronic interactions linked to generalized intra-nuclear cascade, preequilibrium emission and fragmentation models. In addition, FLUKA uses microscopic models for nuclide production that enable particle cascades from prompt and residual radiation to be simulated, together with the Bateman equations for activity build-up and decay radiation calculation. Activity levels induced in patient collimators used in proton therapy have been reported in a few number of works issued by spectrometry or MC calculations [3,7,8]. However, all studies include exclusively pristine Bragg peaks (BP). To our knowledge, realistic beams have not yet been considered, in spite that clinical beams are always modulated.

The two proton therapy centers in France, Centre de Protonthérapie d'Orsay Institut Curie (ICPO) and Centre Antoine Lacassage (CAL) in Nice, share this common problematic. Proton therapy activities started in both centers in 1991, with passive-delivery high and low-energy beams, respectively. Patient-specific devices include ocular collimators in both centers and intracranial and spine collimators and compensators at ICPO. In an independent way, three studies have been carried out in both centers from 2005 to 2017 to determine the isotopes present in activated collimators and their activities, in order to establish appropriate management protocols. Two of them were performed at ICPO in 2005-2007 and 2015, and the last one was carried out at CAL in the period 2015-2017. All studies are based on gamma spectrometry, performed in a total of eight brass collimators irradiated with different proton beams, mostly clinical. MC simulations with the code FLUKA were included in the CAL study. The results of the three studies have been put together and, to complete the work, FLUKA simulations were also performed to calculate ICPO collimator activities. The MC results were compared with experimental data and differences contrasted against those reported in FLUKA benchmark studies. The influence of the modulation and the degradation of the individual monoenergetic beams has been studied in detail. The contribution of the secondary

neutrons to the collimator activation has also been assessed.

In a second step, the correlation of the residual activity with the irradiation parameters was studied from FLUKA simulations for a large set of clinical SOBPs, and from these data a semi-empirical model was derived. The model enables calculation of the activity per isotope and total activity in brass collimators irradiated with any clinical SOBP of a given dose, modulation, range and at a given cooling time longer than 1 month. The FLUKA simulations upon the model is based consider an ideal irradiation with one or multiple monoenergetic beams with no energy spread, so that the real proton fluence, dependent on the characteristics of the beam line, is ignored. The impacts of such simplifications were taken into account and appropriate corrections were proposed as a function of the modulation, degradation and beam line type. The semi-empirical model with the appropriate correction provides a general, practical and fast solution for proton therapy centers to evaluate the residual activities in brass collimators after treatment and its evolution over time.

2. Proton therapy facilities in France

The low energy proton therapy facility at CAL is, since its beginnings in 1991, exclusively devoted to the treatment of mainly ocular tumors, and rarely other ocular diseases. The proton beam is produced at the Medicyc 65 MeV accelerator and reaches the isocenter with energies lower or equal to 62.5 MeV depending on the range required for each patient and quality assurance procedures. The beam line has been described in detail elsewhere [26]. The beam is spread using single scattering passive delivery technique and the field size is limited with several collimators located downstream of the scatterer, ending with a circular field size of 3.4 cm diameter. The patient-specific collimator consists of an 8 mm thick brass disc (CuZn39Pb3, Table 1) with an aperture milled in-house to match the tumor contour. Ocular treatments consist on the irradiation of the tumor volume with a total physical dose of 52 Gy, delivered in four sessions in successive days.

PT center	Brass alloy	Fe	Ni	Al	Cu	Pb	Sn	Others	Zn
CAL (Nice)	CuZn39Pb3	< 0.3	< 0.3	< 0.05	57-59	2.5-3.5	< 0.3	total 0.2	Zn – remainder
ICPO (Orsay)	CuZn39Pb2	< 0.3	< 0.3	< 0.05	59-60	1.6-2.5	< 0.3	total 0.2	Zn – remainder

Table 1. Composition (percent by weight) of collimator brass alloys.

Proton therapy treatments started at ICPO in 1991 with a 200 MeV synchrocyclotron, using double scattering passive delivery technique. The first treatments were devoted to ocular proton therapy from 1991, and intracranial treatments were introduced two years later. In 2010 the old synchrocyclotron was replaced by a 230 MeV IBA cyclotron and a new treatment room with a gantry was built. To treat ocular tumors the beam is degraded down to 77 MeV, and reaches the isocenter with energies up to 73 MeV. The field size at the end of the optical bench is 4 cm diameter. The ocular patient-specific collimator consists of a 1.5 cm-thick brass piece (CuZn39Pb2, Table 1) with a tumor-specific aperture manufactured in-house before the treatment. One of the sides of the collimator has a flange of 6 cm diameter to fix the collimator at the end of the optical bench. The total proton physical dose for uveal melanomas is 54.5 Gy, delivered in four sessions, each session with the same conditions and collimator, as there is a single treatment port. Intracranial treatments are performed at higher energies, up to 230 MeV in the gantry room and up to 200 MeV in the first fix beam line. The proton dose delivered may range from 45 to 74 Gy, and it is delivered in up to 15 sessions using several beams. The patient specific collimator for each beam is also made of the same brass, with a thickness of 5.5 cm to 6.5 cm (gantry) and without flange. The maximum field size is 22 cm.

3. Material and methods

3.1. CAL study

3.1.1. Experimental measurements

For the purpose of this study, two full collimators (3.4 cm diameter brass pieces of 8 mm thickness without aperture) were irradiated with a monoenergetic beam of 62.5 MeV (ID: N_BP1 and N_BP2). Both pieces were irradiated in different dates under equal conditions, with a dose of 13 Gy, which is the dose delivered in one single treatment session for most ocular proton therapy treatments at CAL. A third full collimator was irradiated with the reference SOBP, at a dose of 13 Gy as well (ID: N_SOBP1). The reference SOBP is characterized by a range and a modulation width in water of 32 mm and 16 mm, respectively (proton range is referred in this paper to 90% falloff position). A forth collimator (ID: N_SOBP2) employed in a conventional treatment was also included in the study in order to consider a real clinical case. The last irradiated collimator was also a full collimator (ID: N_SOBP3), irradiated with a low energy beam, fully modulated. The collimators were analyzed with gamma spectrometry at Institute of Chemistry of the University of Nice (ICN), at different post-irradiation times, together with a full collimator which was not irradiated. The cooling times for the different collimators were comprised between 8 days and 2 years. Table 2 summarizes the irradiation and measurement data included in the study.

Spectrometry measurements were performed with an HPGe detector (ORTEC GEM25 vertical detector with 30% intrinsic efficiency, crystal dimensions: 56.8 mm diameter, 56.5 mm thickness, resolution 1.83 keV at 1332 keV, maximal energy 1539 keV) shielded with 5 cm Pb and 1 mm Al for low activity measurements. The irradiated side of the piece was placed against the HPGe detection window. The background radiation was determined for the same measuring time (22 h). The ICN provided the spectra without any data treatment, and the nuclide identification and activity quantification were done by CAL without the use of treatment software and without isotope standard libraries. Besides the energy of the peaks the material composition, possible activation reaction channels and cooling time were also taken into account for nuclide identification.

	Collimator				
ID	**N_BP1**	**N_BP2**	**N_SOBP1**	**N_SOBP2**	**N_SOBP3**
Thickness (cm)	0.8	0.8	0.8	0.8	0.8
Collimator diameter (cm)	3.4	3.4	3.4	3.4	3.4
Aperture surface (cm^2)	0	0	0	1.53	0
Irradiated mass (g)	48	48	48	32	9.6
Maximum energy (MeV)	62.5	62.5	62.5	55	25
Range in water (mm)	32	32	32	26.1	6.2
Modulation in water (mm)	0	0	16	14.6	6.2
Proton dose (Gy)	13	13	13	52 (4 fract.)	55
Last irradiation date	2015/05/28	2014/09/22	2017/01/23	2017/01/20	2017/09/15
1^{rst} measurement date	2015/06/23	2015/06/23	2017/01/31	2017/02/01	2017/09/26
1^{rst} cooling time	25 d	9 m	8 d	11 d	11 d
2^{nd} measurement date	2016/09/06	2016/09/12	-	-	-
2^{nd} cooling time	15 m	2 y	-	-	-

Table 2. Irradiation and measurement data from CAL study.

In the case of the pristine Bragg peak (BP) irradiations, the total activity and specific activity measured for a given radionuclide, A_i and A_{mi}, respectively, expressed in units of Bq and Bq/g respectively, were determined as follows:

$$A_i(Bq) = \frac{N_i}{Ef.T_m.Br} \quad (1)$$

$$A_{mi}(Bq/g) = \frac{A_i}{m_i} \quad (2)$$

where N_i is the peak count of nucleus *i*, *Ef* is the full-energy peak efficiency, T_m the measuring time, *Br* is the gamma-ray emission rate and m_i is the irradiated mass. The irradiated mass was calculated considering the irradiated area of the collimator, the proton path in brass provided by the experimental software SRIM (SRIM-2013.0) [27] and the brass density.

Peaks lower than two-fold the background noise were not considered, as it is not possible to distinguish at such low levels real peaks from background fluctuation.

The full-energy peak efficiency provided by the spectrometry laboratory is shown in equation 3 and was experimentally determined from a 27.67g sample of certified reference material IAEA-385 [28] enclosed in a 5 cm-diameter cylindrical plastic box.

$$Ef(E) = exp\left(\frac{-12.21+\frac{99.33}{ln(E)}+\frac{-228.62}{ln^2(E)}}{1+\frac{-2.06}{ln(E)}}\right) \quad (3)$$

where *E* is the energy in keV. The IAEA-385 reference material is a sample of Irish sea sediment, composed of Si, Ca, Al, Fe, K, C and N, with a density of 2.65 g/cm^3 [29]. In order to take into account the differences between the reference material and the brass full collimators (geometry, density, and self-absorption), appropriate correction was applied to the efficiency curve. The correction was determined by MC simulation using the code MCNP6 [30]. Two set of simulations were performed: in the first set we calculated the efficiency of a simple detector, consisting on a 1 mm thick and 5.68 cm diameter disc made of air, in front of which a brass cylinder simulating the full collimator was modelled (8 mm thick, 3.4 cm diameter, 8.4 g/cm^3). The piece was separated from the detector by 1 mm. A volumetric homogeneous photon source was modelled inside the collimator, on the closest side to the detector, from its surface down to a depth equal to the 62.5 MeV proton beam path in brass, and covering the whole collimator transversal section. The source was isotropic and monoenergetic. Only photons were transported (mode p). For a given energy E_i, the efficiency was calculated as the ratio of the photon flux averaged over the detector volume to the photon flux averaged over the source volume. Fluxes were calculated with tally f4, in an energy window of $E_i \pm 1$ keV. The described geometry was the same for all simulations, each simulation with a different photon source energy, covering the range from 2 to 2000 keV (31 simulations per set). In the second set of simulations the efficiency of the reference material sample (IAEA-385) was similarly calculated. In this case the source was replaced by a disc of sediment material, with geometry, density and composition set to previous descriptions. The efficiency was calculated for the same set of energies. The efficiency curve given by the spectrometry laboratory for the reference material, *Ef*, was then corrected by multiplying the curve by the ratio of the efficiency of brass full collimator (e_{BFC}) to that of the reference material ($e_{IAEA\text{-}385}$), for the whole energy range (equation 4).

$$Ef_{BFC}(E) = Ef(E)\frac{e_{BFC}(E)}{e_{IAEA-385}(E)} \quad (4)$$

3.1.2. Monte Carlo simulations

Calculation of the activity for the irradiated full collimators was performed with the code FLUKA (version 2011.2c.0) [31,32] and the user interface Flair (version 2.1-1) [33]. The geometry was reduced to the final full brass piece previously described. The material composition was set to that of CuZn39Pb3 alloy, considering impurities as well. The external dimensions were modeled according to real ones and always without aperture, even in the case of collimator N_SOBP2. To score the residual nuclei and their activities, the card *RESNUCLEI*, associated to one or several cooling times and to one or several cells (i.e. the collimator) through the *RADDECAY* and the *DCYSCORE* cards, was used. The *RESNUCLEI* card yields a list of isotopes induced in the material selected, together with the activity and the relative error. Spallation and low energy neutron residuals were scored separately. All relevant cards recommended for activation calculations in FLUKA were activated: the

DEFAULTS card was set to *PRECISION* (defaults for precise simulations) *and the COALESCENCE* (coalescence mechanism) and *EVAPORATION* cards (evaporation model with heavy fragment evaporation) were switched-on. The low energy neutron transport was activated through the *LOW-NEUT* option.

The specific activity was calculated with the irradiated mass. The irradiation profile and parameters were set to match the experimental ones. A cooling time of 1 month was selected. For collimators N_BP1 and N_BP2, the beam energy was set to 62.5 MeV (with no energy spread), the irradiation time to those employed in the experiences (around 4 seconds) and the number of protons N was calculated from the beam flux φ at the surface of the piece and the irradiated area of the collimator, S_{colli} (equations 5 and 6).

$$N = \varphi . S_{colli} \quad (5)$$

$$\varphi\ (cm^{-2}) = \frac{D_0}{\frac{S}{\rho}.1.602.10^{-10}} \quad (6)$$

where S/ρ is the proton stopping power in water in MeV·cm^2/g for a proton energy of 62.5 MeV and D_0 is the entrance dose in Gy (2.6 Gy).

For collimators N_SOBP1, N_SOBP2 and N_SOBP3, induced activities were calculated with FLUKA for each individual peak conforming the SOBP, by using the previously described method. For each simulation only the input energy was accordingly modified. The total activity from the SOBP was calculated following equation 7:

$$A_{SOBP}(Bq) = \sum_i \sum_n (A_{i,n} * p_n) \quad (7)$$

where *i* stands for isotope *i* and p_n is the weight coefficient for the BP *n*. The set of weighting coefficients p_n were adjusted such as to have a flat plateau of the required dose.

In the case of N_BP1, N_BP2 and N_SOBP1 collimators, the total and specific activities, both experimental and calculated, were multiplied by 4 whenever required for comparison purposes, to refer the results to a therapeutic dose (52 Gy in 4 sessions of 13 Gy/session). This approximation is acceptable because the study is focused on the long-term management and is thus aimed at isotopes with relatively long half-life.

The impact of using the described simplified geometrical model together with a monochromatic source without energy spread is evaluated in section 3.3.

3.2. ICPO studies

3.2.1. Experimental measurements

The first study carried out at ICPO was ordered to the Commissariat à l'énergie atomique (CEA) and included gamma spectrometry with, among others, an ocular patient-specific collimator (ID: N_SOBP1) employed in a treatment. Other collimators comprised in the study were not included in this paper due to missing data. The ocular collimator and irradiation characteristics are reported in Table 3. The spectrometry measurements were performed *in situ* with a gamma spectrometry chain composed of a portable and collimated GeLi detector (CANBERRA, 40% intrinsic efficiency), an Inspector 2000 dispositive to acquire and code the impulsions and a portable PC with the data treatment software. The activity determination was made with the software ISOCS (In Situ Object Counting System), which takes into account the combination of the detector properties, the measurement geometry, the composition, and shape of the measured material (density and geometry) to establish an efficiency curve adapted to the measurement. This system avoids the use of any calibration reference source. The measurement acquisition was 20.5 hours.

The second study carried out at ICPO in 2015 on the activation of ocular and intracranial collimators was also performed with spectrometry analysis. For the purpose of the study, an ocular collimator (ID: O_SOBP2) and two intracranial collimators (IDs: O_SOBP3 and O_SOBP4), all of them used in treatments, were selected. In addition, one collimator not irradiated was used to determine the background and possible radionuclides initially present. The spectrometric analyses were performed at the Institute de Physique Nucléaire d'Orsay (IPN) with an HPGe spectrometer (model GC4019-7500SL, Canberra). Activities were calculated from the number of counts for each energy peak convolved by the efficiency curve of the spectrometer. The efficiency curve was obtained for a SG500 source, which is based on a cylinder (4.7 cm radius, 7.2 cm long) of near water equivalent material with several radionuclides of a known activity. No correction was applied to take into account the composition and shape of the analyzed pieces. The measurement acquisition time ranged from 8.5 to 20.6 hours depending on the piece. The analyses were performed at different post-irradiation times, from 11 days to 4.3 years. The nuclide identification was based on standard libraries. Three radionuclide rejection criteria were applied: 1) $T_{1/2}$<10 days, 2) less than 40% of the energy lines of a given radionuclide detected in the spectrometric study, 3) unfulfillment of the interference analysis. Table 3 summarizes the data of the two ICPO studies.

	Collimators			
ID	**O_SOBP1**	**O_SOBP2**	**O_SOBP3**	**O_SOBP4**
Thickness (cm)	1.5	1.5	5.5	5.5
Collimator diameter (cm)	4	4	7	7
Aperture surface (cm^2)	1.10	1.43	10.4	9.70
Irradiated mass (g)	48.1	43.1	495	339
Maximum energy (MeV)	55	52.5	125	100
Range in water (cm)	2.60	2.32	11.3	7.90
Modulation in water (cm)	1.18	2.32	6.81	4.01
Proton dose (Gy)	54.5 (4 fractions, 13.6 Gy/fraction)	54.5 (4 fractions, 13.6 Gy/fraction)	4.1 (5 fractions, 0.8 Gy/fraction)	3.3 (2 fractions, 1.6 Gy/fraction)
Last irradiation date	2003/04/15	2010/11/26	2012/01/13	2015/03/13
Measurement date	2005/11/18	2015/03/26	2015/03/26	2015/03/26
Cooling time	2.5 y	4.3 y	3.1 y	11 d

Table 3. Properties of collimators irradiated and analyzed at ICPO.

As in the case of the CAL study, the calculation of specific activities from the total activities was made by considering the irradiated mass instead of the total mass.

3.2.2. Monte Carlo simulations

Collimator activities were also simulated with FLUKA using the same version and method as those employed for CAL collimators (section 3.1.2). SOBP activities were therefore computed from activities of all individual BPs conforming the SOBP, as previously described (equation 7). The total activity was calculated using the same geometry and beam field as those for the CAL collimators, except for the intracranial collimators for which the brass thicknesses were increased to 5.5 cm. The specific activities were finally calculated considering the irradiated mass of each collimator according to their real dimensions and to the beam size.

3.3. Impact of the simplifications of the FLUKA model

The FLUKA simulations described in sections 3.1.2 and 3.2.2 consider an ideal collimator irradiation: the simplistic geometrical model includes only the collimator and hence does not take into account the real proton spectral fluence dependent on the beam line design and components of the nozzle, such as the degrader. The model ignores also the neutron component created upstream of the collimator and impinging on it, whose amount and spectral fluence will likewise be dependent on the beam line. The description of the source, a monoenergetic proton beam without energy spread, does not make up for the absence of the beam line components in the model. These choices were consciously made in order to consider a baseline case useful for any clinical proton beam irradiation. However, the implications of the simplifications must be assessed in order to evaluate their impact.

To estimate the influence of the proton beam energy spread and the neutron secondary field on the collimator activation, comparative simulations were done with the simple model and with a realistic one. In the realistic model, the whole CAL optical bench of the proton therapy beam line was modeled in the geometry. The source was placed right after the Kapton foil that isolates the part of the beam line kept under vacuum pressure. The beam loses the energy in its path through the air, down to 62.5 MeV at the level of the isocenter. The source, located before the layer, was the same for all simulations (65 MeV). The irradiation profiles and number of protons were set to arbitrary equal values. Both models were run at 10, 20, 40 and 62.5 MeV energies, adding, in the case of the realistic model, the required Plexiglass thickness at the position of the modulator. On both realistic and simple models an air cell was added right upstream of the collimator to score the proton spectral fluence, and the spallation and low energy neutron activities at one month cooling time were scored in the collimator, following the same methodology previously reported. The activities were corrected by the proton fluence impinging on the surface of the collimator. The neutron fluence was also scored in the collimator for the energy of 62.5 MeV in the two models. For the sake of comparison, these last simulations were also performed with the code MCNP6 [30].

3.4. Semi-empirical model for residual activity calculation from proton irradiation in brass collimators

Activities in brass collimators at 1 month cooling time were calculated with the FLUKA simple model, previously described, for a set of monoenergetic beams ranging from 5 to 250 MeV, in steps of 5 MeV, covering the range of energies used in proton therapy. The corresponding depth dose distributions in water were also calculated for each energy. All simulations were performed with the same arbitrary number of protons (5E10). The total specific activity was calculated from the sum of all residual isotopes with activities above 1% of the total activity, at any energy and for cooling times of 1 and 6 months and 1, 2 and 5 years. The data points of individual and total specific activities as a function of beam energy were fitted to a 6-degree polynomial function. From the depth dose distributions of individual monoenergetic beams we generated up to 75 different SOBPs, with different modulations (from pristine BPs to fully modulated SOBPs), maximum energies (50 MeV, 100 MeV, 150 MeV, 200 MeV and 250 MeV) and doses (1-110 Gy). For each SOBP, the ponderation coefficients p_n to obtain a flat plateau of the chosen dose were calculated, which were applied to equation 7 to calculate the SOBP specific activities, both for individual isotopes and total amounts. The relationship between the SOBP beam parameters and the specific activity was studied from these data. The semi-empirical model was developed from the correlation of the specific activity A_m (both for individual isotopes and total amounts) and the SOBP modulation M, range R and dose D. All data fits were done with R [34].

The impact of the simplified FLUKA simulations used on the semi-empirical model (section 3.3), was considered to propose

general correction factors on the specific activities yielded by the model as a function of the modulation, degradation and beam line type.

4. Results

4.1. Experimental and calculated specific activities

Fig. 1 shows three of the gamma spectra obtained in the CAL study (N_BP1, N_SOBP1 and N_SOBP3), corrected for efficiency. The efficiency for brass full collimators was approximately two-fold the efficiency curve provided by the spectrometry laboratory for the IAEA-385 reference material, and this factor had relatively little dependence on the energy (1.8-2.4). The peak at 1.46 MeV was present both in the non-irradiated collimator and in the background spectrum, and is associated to K-40, from natural telluric radiation. It is thus part of the background radiation measured by the HPGe detector. Other minor peaks were also present in both irradiated and non-irradiated collimators, and were not considered.

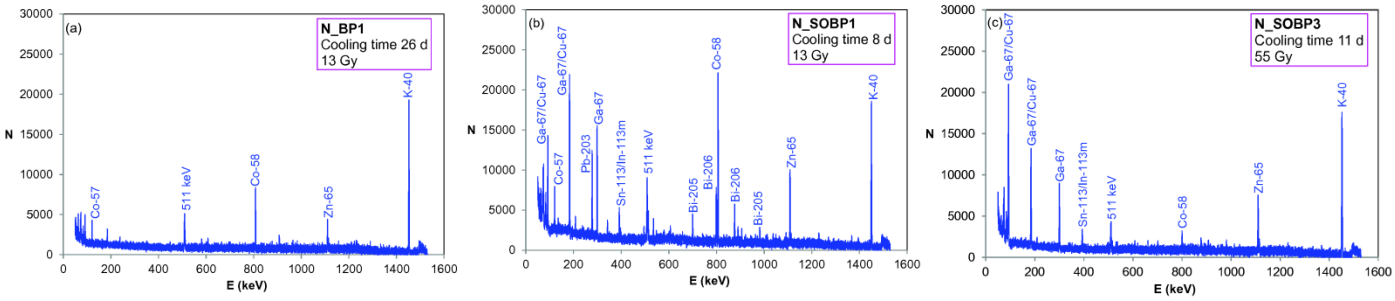

Fig. 1. Gamma spectra in counts N, corrected for efficiency, for (a) N_BP1, at 1 month cooling time irradiated with a pristine BP, 13 Gy; (b) N_SOBP1 at 8 days cooling time, irradiated with the reference SOBP, 13 Gy and (c) N_SOBP3 at 11 days cooling time, irradiated with a fully modulated beam, 55 Gy.

For BP irradiations, only Co-57, Co-58 and Zn-65 were identified in irradiated collimators and were not found in the non-irradiated one. Besides these, many other peaks appeared in collimators irradiated with modulated beams of the same range, identified as those of Ga-67, Pb-203, Sn-113/In-113m, Bi-205, Bi-206 and possibly Cu-67. Cooling times employed for modulated beams were generally shorter (about 10 days) than those of pristine BPs (>1 month); therefore isotopes with short half-life such as Ga-67 (3 d), Pb-203 (2 d), Bi-206 (6 d) and Bi-205 (15 d) may have decayed after 1 month. The peaks at 93 keV and 185 keV might come both from Ga-67 and Cu-67. However, the quantification of Cu-67 based on the activity of Ga-67 derived from the 300 keV peak was inconsistent between the two peaks. The quantification in the low energy range (<100 keV) is indeed associated to a larger uncertainty because the efficiency curve varies drastically in this energy range. Therefore, Cu-67 could not be quantified and Ga-67 activity was derived only from the 300 keV peak. All identified isotopes were known activation products mostly produced in (p,X) and (n,X) reactions. In the case N_SOBP3, irradiated with a fully modulated beam of lower maximum energy (25 MeV), Co-57, Bi-205, Bi-206 and Pb-203 were not present. This is consistent with the higher energy yields of proton activation cross-sections for these products. Finally, the intensity of the peaks also responds to the delivered dose, as observed by comparison of N_SOBP1 and N_SOBP3 spectra (Fig. 1b and 1c).

Fig. 2 shows the decay curves for the most relevant isotopes issued from MC calculation for the CAL BP irradiation, along with the experimental results at 1 (N_BP1, first measurement), 9 (N_BP2, first measurement) and 15 months (N_BP1, second measurement). The second measurement of N_BP2 collimator, at 2 years post-irradiation, yielded no activity over background noise.

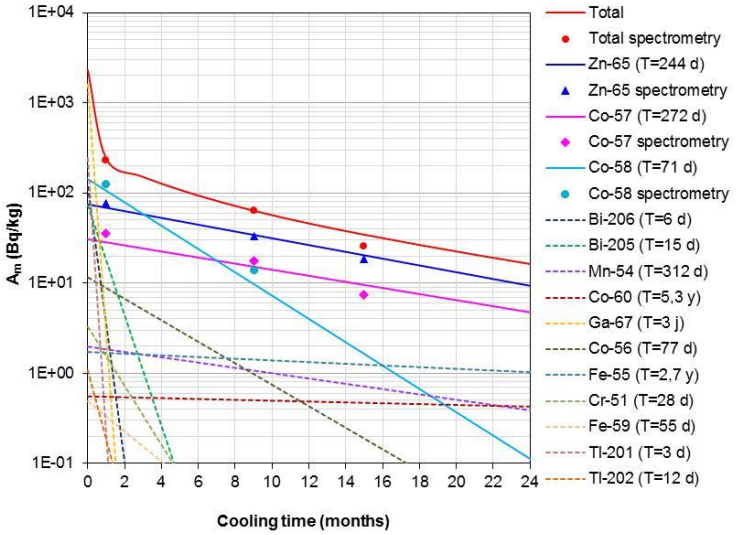

Fig. 2. Decay of total calculated specific activity and specific activity per radionuclide for the CAL BP irradiation, 52 Gy. Experimental points from spectrometry measurements are also shown.

The decay curves calculated with FLUKA for the monoenergetic beam closely match experimental points at different cooling times (Fig. 2), even if comparatively higher differences were obtained for individual isotopes at longer cooling times. Note that MC total activity is the sum over the whole list of isotopes shown in the figure; therefore the agreement for total activities depends also on the number of isotopes detected with spectrometry. The higher differences at longer cooling times are attributed to experimental uncertainties, which rise as activity levels fall to background noise. On the other hand, isotopes with very low energy emissions (e.g. Fe-55) or very low activities (e.g. Mn-54) could not be detected with spectrometry, since such low activities are of the order of the background spectrum. Likewise, isotopes with very short half-lives with respect to the cooling time at measurement date (e.g. Ga-67) were neither detected.

As in the case of CAL study, some energy lines were detected in the ICPO background collimator but could not be attributed to any radionuclide. All energy lines detected in the irradiated ICPO collimators and not present in the background collimators were identified as proton activation radionuclides.

The list of relevant nuclides from activation in CAL and ICPO collimators determined from FLUKA and spectrometry analysis is shown in Table 4. The experimental and calculated specific activities were all referred to 1 month post-irradiation and, in the case of N_BP1 and N_SOPBP1 collimators, activities were referred to 52 Gy to facilitate comparison with the other collimators. The ratios between the experimental measurements and the FLUKA calculations are also provided.

		A_m(Bq/kg) referred to 1 month post-irradiation									
Collimator	**Isotope**	**Co-57**	**Co-58**	**Zn-65**	**Ga-67**	**Bi-205**	**Bi-206**	**Mn-54**	**Co-56**	**Co-60**	**Total**
	$T_{1/2}$ (d)	272	71	244	3.3	15	6	312	77	1925	
N_BP1 (52 Gy)	**Exp.**	35.4	119	74.8							229
	FLUKA	26.7	116	76.0	2.97	20.4	4.0				246
	Exp./FLUKA	1.33	1.03	0.98							0.93
N_SOBP1 (52 Gy)	**Exp.**	59.6	432	476	12.0	123	19.2				1122
	FLUKA	64.6	300	218	9.12	59.8	12.2				664
	Exp./FLUKA	0.92	1.44	2.18	1.32	2.06	1.57				1.69
N_SOBP2 (52 Gy)	**Exp.**	27.4	309	417	6.67	129	30.8				920
	FLUKA	47.2	253	228	10.5	63.5	14.7				616
	Exp./FLUKA	0.58	1.22	1.83	0.63	2.03	2.25				1.49
N_SOBP3 (55 Gy)	**Exp.**			460	24.8		11.3				496
	FLUKA		0.03	144	9.31	60.0	8.8				185
	Exp./FLUKA			3.19	2.66		1.28				2.68
O_SOBP1 (55 Gy)	**Exp.**	183		809							992
	FLUKA	51.0	270	237				2.78	15.3		576
	Exp./FLUKA	3.59		3.41							1.72
O_SOBP2 (55 Gy)	**Exp.**			1128							1128
	FLUKA	42.6	242	253				2.2	10.9		551
	Exp./FLUKA			4.46							2.05
O_SOBP3 (4.1 Gy)	**Exp.**	42.6		115				15.6		3.41	177
	FLUKA	21.4	63.4	22.7				2.47	17.6		128
	Exp./FLUKA	1.99		5.07				6.32			1.38
O_SOBP4 (3.3 Gy)	**Exp.**	9.68	66.0	70.6				1.78	8.84	0.76	158
	FLUKA	9.91	32.4	14.0				0.92	7.25		64
	Exp./FLUKA	0.98	2.04	5.04				1.93	1.22		2.45

Table 4. Experimental and calculated activities from gamma spectrometry and FLUKA referred to one month post-irradiation for CAL and ICPO collimators.

The ratios of experimental activities over those calculated with FLUKA yielded in the CAL study for the monoenergetic beam are close to 1 except for Co-57 (1.33). The differences are larger for collimators irradiated with modulated beams, for which calculations, except for one value (Ga-67 in N_SOBP2 collimator), systematically underestimate the activities of all but Co-57 nuclides. The differences for Co-57 do not look systematic. The growing differences for higher modulations can be observed specially for Zn-65: for half-modulated beams (N_SOBP1 and N_SOBP2) the ratio is about 2, whereas for N_SOBP3, irradiated with a fully modulated low energy beam (< 25 MeV) the ratio increases to more than 3.

The ICPO nuclide inventory at 1 month post-irradiation is consistent with that of CAL for ocular collimators (Zn-65, Co-57 and Co-58), except for Bi-205 which was not reported in collimator O_SOBP4 (Bi-206 does not fulfill the half-live criterion); the others were analyzed at too long cooling times. For high energy treatments, Mn-54, Co-56 and Co-60 were additionally detected. The activation cross sections for these three isotopes have indeed higher energy yields and are lower at intermediate energies. In contrast with CAL experimental results, the total or a large amount of the total experimental activities in ICPO collimators come from Zn-65, especially in the case of ocular collimators. The reason for three of the collimators (O_SOBP1, O_SOBP2 and O_SOBP3) is that spectrometric analyses were performed at too long post-irradiation times (>2.5 years) with respect to the half-lives of the present isotopes. This is especially the case of Co-58 ($T_{1/2}$=71 d) for the three collimators and also of Co-56 ($T_{1/2}$=77 d) and Co-57 ($T_{1/2}$=272 d) for O_SOBP2 and O_SOBP3 collimators, respectively. The underestimation of experimental activities reported for CAL collimators irradiated with an SOBP, particularly for Zn-65, was also found here but with a larger underestimation (3.4-5.1). Only a higher difference was obtained for Mn-54 in the case of O_SOBP3 collimator (ratio of 6.3), which is not consistent with that of O_SOBP4, irradiated under similar conditions. The experimental result in the first case is linked to a higher error due to both the low

production rate of Mn-54 with respect to the other activation products, and especially to the much longer cooling time at measurement (more than 3 years with respect to 11 days). In general, for high energy beams ratios are greater than for ocular beams. It should be noted that the ratios between total experimental activities and total FLUKA activities do not always look consistent with ratios for individual isotopes, which rise up to 5, because the number of isotopes is different in spectrometry analyses and FLUKA.

4.2. Impact of the simplifications of the FLUKA model

Fig. 3a shows the proton relative fluence upstream of the collimator for the realistic model at 10, 20, 40 and 62.5 MeV. The effect of the degrader on the proton energy spectra can be observed for the 10, 20 and 40 MeV beams. The spread is logically wider as thicker is the degrader and the shape of the distributions is consistent with measured and simulated spectral proton fluences published elsewhere [35].

Fig. 3b compares the neutron spectra from the simple and the realistic models for the non-modulated beam. Neutron fluences yielded by FLUKA and MCNP6 were fully consistent. The results show that low energy neutrons (<meV) are not produced in the simple model, whereas the spectrum extends down to thermal energies in the case of the realistic geometry. In spite of this, the intermediate and thermal components of the spectrum are negligible with respect to the high energy peak from evaporation and spallation neutrons.

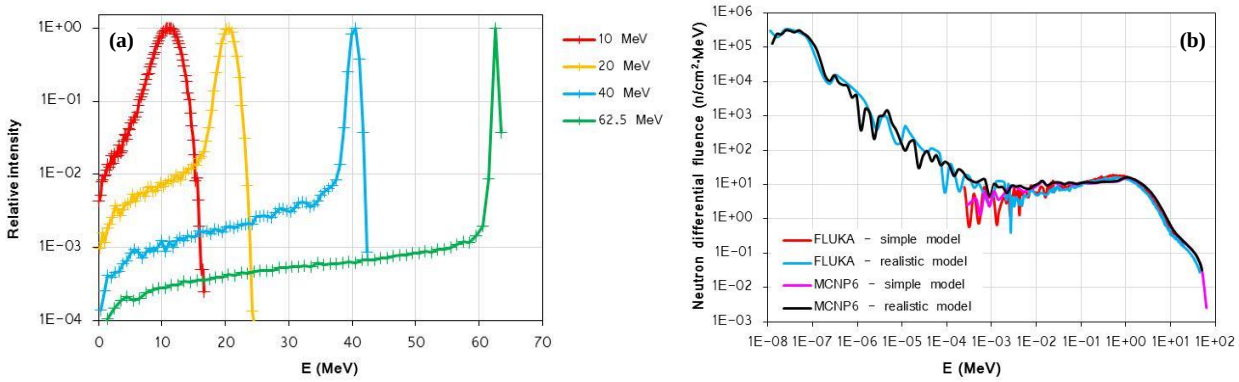

Fig. 3. (a) FLUKA relative proton fluence impinging on the collimator issued from the realistic model, for an initial beam of 65 MeV (62.5 MeV after the air gap) degraded down to energies of 10, 20 and 40 MeV. (b) FLUKA and MCNP6 neutron spectra in the collimator for a non-modulated beam of 62.5 MeV, for both the realistic and the simple models.

The realistic model yielded an activity of Zn-65 1.2-fold larger than the simple for an energy degradation of 10 MeV, and this ratio decreased with thinner degraders down to unity, for null degradation. Almost all the Zn-65 activity was scored in the spallation tally with less than 1% in the low energy neutron component. These results show that the degradation of the beam, that modifies the spectral proton fluence, has a non-negligible impact on the activation (up to 20% for Zn-65 with high degradations). For SOBPs the impact will grow with the modulation because of cumulative effect of multiple degraded beams. In opposition, the neutron contribution generated upstream of the collimator has a negligible contribution to the total activity and hence its omission in this type of calculations is acceptable for beam lines with similar or lower neutron production. For the other activation products the effect is less noticeable because the production energy yields of possible proton activation reactions are either higher or less probable. The production of Zn-65 via ^{65}Cu(p,n)^{65}Zn reaction has both a very low energy yield (about 2.5 MeV) and a non-negligible cross section (of the order of 1 b). This fact explains that differences between FLUKA and experimental activities are higher for Zn-65, especially for modulated and degraded beams.

4.3. Semi-empirical model for residual activity calculation from proton irradiation in brass collimators

The FLUKA simulations described in section 3.3 provided the individual and total activities as a function of the beam energy. The isotopes considered in the calculation of the total activity, according to the described criterion, were Bi-206, Bi-205, Zn-65, Co-58, Co-57, Co-56, Fe-55, Mn-54, Mn-52, Ga-67 and Cr-51. Fig. 4a shows the relative activity of each isotope as a function of the beam energy. The 6-degree polynomial function used to fit the total activity to the energy was used to calculate the activities of up to 75 SOBPs of different doses, modulations and maximum beam energies, using the ponderation of individual BPs conforming the SOBPs. For a given energy, the total specific activity over the dose, A_m/D, was found to be correlated to the modulation and the range of the SOBP, expressed as the ratio M/R. More particularly, data points were fitted to a nonlinear regression model based on the Michaelis-Menten function, with the term of M/R in the denominator modified by a power *d* to enhance the fit.

$A_m/D = a + \frac{b*M/R}{c+(M/R)^d}$ (8), expressed in units of Bq/g·Gy, where

$a = (A_m/D)_{min} = (a_1E^2 + a_2E + a_3)$ (9)

$b = (b_1E^2 + b_2E + b_3)$ (10)

The coefficients *a* and *b* are related to the maximum and minimum activations and only depend on the maximum beam energy and dose. The coefficient *a* is exactly the minimum activation. However, unlike in the Michaelis-Menten function, the

sum of *a* and *b* is not the maximum activation, but higher. This is because the Michaelis-Menten function is asymptotic, whereas equation 8 takes a maximum value at M/R equal to 1. The maximum activation was found to be a linear function of the energy (Eq. 11).

$(A_m/D)_{max} = (2.23{\cdot}10^{-4}E + 4.84{\cdot}10^{-4})$ (11), in units Bq/g·Gy.

Coefficients *c* and *d* varied little and were not found to be correlated with the energy. They were thus both set to the mean value over energies. As a result, equation 8 fits better at some energy than other (Fig. 4b). Like in Michaelis-Menten function, the coefficient *c* is actually the value of M/R at half incremental A_m/D (Eq. 12).

$c = \frac{\Delta(A_m/D)}{2} = \frac{(A_m/D)_{max} - (A_m/D)_{min}}{2}$ (12)

Fig. 4b shows the FLUKA data points of the activity over the dose as a function of the modulation (M/R) for several energies from 50 to 250 MeV, where the curves in blue were obtained from equation 8, and the data points corresponding to the collimators irradiated at CAL and ICPO are also shown.

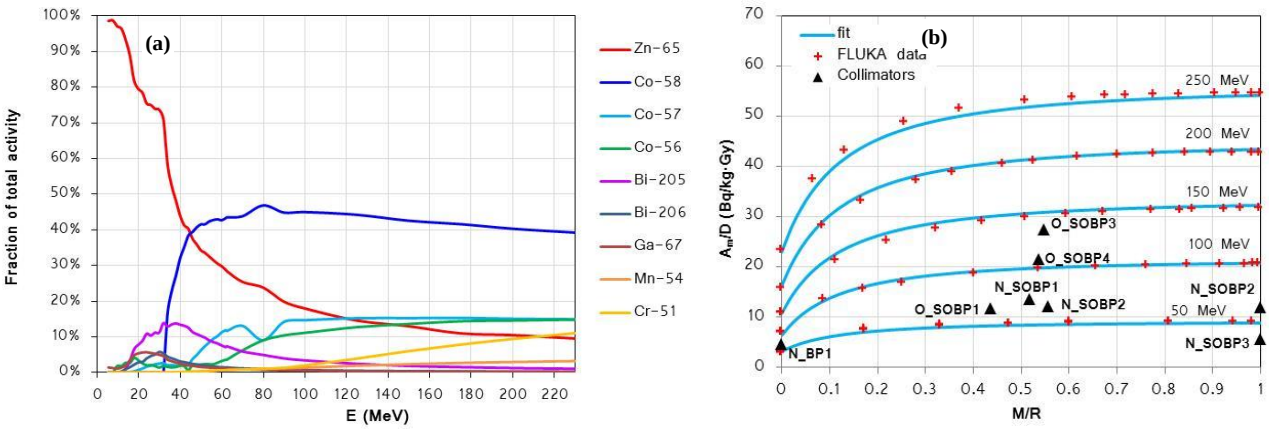

Fig. 4. **(a)** Activity fractions per isotope as a function of beam energy at 1 month cooling time. **(b)** A_m/D (1 month cooling time) as a function of modulation M/R, for energies from 50 MeV to 250 MeV, calculated with FLUKA (red cross) and fitted with a non-linear regression model based on the Michaelis-Menten function. Experimental data for brass collimators included in the CAL and ICPO studies are also plotted.

Table 5 shows the comparison of activities calculated with the semi-empirical model and the experimental data.

Collimator	m (g)	E (MeV)	M* (mm)	R* (mm)	M/R	D (Gy)	A_m/D (Bq/kg·Gy)	Semi-emp. model A (Bq/kg)	Experimental A (Bq/kg)	Ratio Exp./analyt.
N_BP1	48	62.5	0	32	0.00	52	4.62	205	229	1.1
N_SOBP1	48	62.5	16	32	0.50	52	13.5	587	1122	1.9
N_SOBP2	32	55	14.6	26.1	0.56	52	12.1	504	920	1.8
N_SOBP3	9.6	25	6.2	6.2	1.00	55	5.65	154	496	3.2
O_SOBP1	48.1	55	11.8	26	0.45	54.5	11.8	517	992	1.9
O_SOBP2	43.1	52.5	23.2	23.2	1.00	54.5	12.0	518	1128	2.2
O_SOBP3	495	125	68.1	113	0.60	4.1	27.5	105	177	1.7
O_SOBP4	339	100	40.1	79	0.51	3.3	21.6	65	158	2.4

Table 5. Characteristics of the irradiations and collimators from CAL and ICPO studies, and comparison of total activities issued from the semi-empirical model and the spectrometry at 1 month cooling time. *The modulation M and range R refer to water.

The specific activities calculated from the semi-empirical model are logically in agreement with experimental values, within the ratios directly obtained with FLUKA (Table 4). The higher differences yielded for some individual isotopes, up to a factor of about 5 (Table 4), are not visible here because they are compensated by the fact that the total activity is calculated from 11 isotopes, whereas the total activities from spectrometry are due to less than those.

With appropriate coefficients, equations 8-12 are also applicable to most of the individual isotopes. In the case of Bi-205, Bi-206 and Ga-67, data points did not properly fit to a unique equation because of more complex functions of activity with the energy, showing a sharp growth at low energies followed by a softer slope at higher energies. Nevertheless, these are the three isotopes with shortest half-lives (15, 6 and 3 days respectively) and thus less relevant as regards radioactive waste management issues. Mn-52 was also discarded provided its very short half-live (5 d) and low contribution to total activity in all energy range. For the remaining isotopes, individual specific activities were fit to a 6-degree polynomial function, and the coefficients were determined following the same method. Table 6 shows the coefficients of equations 8-12 for total and individual specific activities. Equations are only valid at energies above the cutoff energies of the involved activation cross sections, indicated on the last column. The minimum energies were derived from the curves of the activities as a function of energy, for individual isotopes and total amounts (Fig.4a). The use of equations for energies below those indicated yields negative activities or activities decreasing with modulation.

Isotope	a_1	a_2	a_3	b_1	b_2	b_3	c	d	$T_{1/2}$	Min. E (MeV)
Zn-65	1.823E-08	-4.366E-07	1.073E-03	4.846E-08	1.728E-05	2.236E-03	1.483E-01	0.979	244 d	5
Co-56	1.779E-08	1.104E-05	-5.277E-04	-4.631E-08	4.077E-05	-1.985E-03	6.950E-02	1.002	77 d	55
Co-57	1.288E-08	1.186E-05	-3.703E-04	-8.610E-08	5.143E-05	-2.097E-03	1.251E-01	1.099	272 d	45
Co-58	4.791E-08	2.438E-05	-5.000E-06	-2.695E-07	1.410E-04	-4.221E-03	1.348E-01	1.082	71 d	35
Mn-54	1.495E-08	-5.990E-07	6.600E-06	8.114E-09	3.243E-06	-1.894E-04	1.035E-01	1.108	312 d	55
Cr-51	8.315E-08	-1.053E-05	3.459E-04	8.143E-08	-5.123E-06	1.813E-05	1.038E-01	1.120	28 d	60
Fe-55	1.005E-08	7.389E-08	-9.160E-06	8.954E-10	4.259E-06	-2.054E-04	1.127E-01	1.070	2.7 y	50
Total*	2.331E-07	2.907E-05	1.209E-03	-3.499E-07	2.491E-04	-5.191E-03	1.300E-01	1.049	Eq.15	15

Table 6. Coefficients for calculation of individual and total activities (in Bq/g·Gy) from equations 8-12 and 15, half-lives and range of validity of equations (minimum energy). *From Bi-206, Bi-205, Zn-65, Co-58, Co-57, Co-56, Fe-55, Mn-54, Mn-52, Ga-67 and Cr-51.

To calculate A_m/D of an individual isotope for a cooling time longer than one month, equation 8 should just be corrected by the decay law, with its half-life:

$$(A_m/D)_t = (A_m/D)_{1m} exp(-\lambda_i t) \quad (13)$$

where *t* is the time elapsed from one month cooling time, $(A_m/D)_{1m}$ is A_m/D of isotope *i* at one month given by equation 8, and

$$\lambda_i = \frac{ln2}{T_{\frac{1}{2}i}} \quad (14)$$

To extend the use of equation 8 for total activity to longer cooling times, without need to calculate all individual activities, the curves from equation 8 were also calculated at 6 months, 1 year, 2 years and 5 years. From the data, an effective half-life $T_{1/2eff}$ dependent both on the energy and on the cooling time was determined for the total activity:

$$T_{1/2eff} = (k_1 E^2 + k_2 E + k_3) t^2 + k_4 t + k_5 \quad (15)$$

with k_1=-3.030E-08, k_2=1.146E-05, k_3=-1.948E-03, k_4=0.1606 and k_5=2.722, and *t* expressed in months.

Since the semi-empirical model is based on perfect monochromatic beams, it is valid, without further correction, for non-degraded pristine BPs delivered with beam lines with intrinsically low energy spread. For other general cases the activities will be underestimated to different extents depending on the degree of modulation and degradation, and on the beam line characteristics. For modulated beams, a correction factor of 2 was calculated from the mean differences obtained between FLUKA and spectrometry (section 4.1) and is recommended both for total activities and for isotopes other than Zn-65. In the case of Zn-65, more impacted by beam degradation, modulation and beam line design, the correction factor was carefully studied as a function of these parameters, based on the characteristics of the beams studied and on the results obtained. The following factor was found to suitably correct the differences observed:

$$F_{Zn-65} = F_D \cdot F_M \cdot F_B \quad (16)$$

where F_D, F_M and F_B account, respectively, for the effects of the degradation, modulation and beam line type, and may be calculated as follows:

$$F_D = 1 + \frac{E_i - E_m}{E_i} \quad (17)$$

with E_i the initial energy of the beam without degradation and E_m the maximum energy of the irradiation (degraded beam),

$$F_M = \begin{cases} 2 for\ M/R > 0.45 \\ 1 for\ M/R < 0.45 \end{cases} \quad (18)$$

and F_B=1 for beam lines with intrinsically low energy spread and F_B=2 for beam lines with intrinsically high energy spread (e.g. double scattering system). Application of this correction factor (with F_B=1 for CAL and F_B =2 for ICPO) provides activities of Zn-65 much closer to experimental results for all collimators analyzed in this work (factors 0.6-1.3 instead of 1.3-5.2).

5. Discussion

Isotopes produced in brass collimators are mostly generated via (p,X) and (n,X) reactions on copper, zinc and lead nuclei and fall in the region of mass A=60 (copper and zinc) and A=200 (lead). Gamma spectrometry performed at cooling times from about 10 days to 4 years on ocular and intracranial collimators showed the presence of mainly Co-58 (71 d), Zn-65 (244 d) and Co-57 (272 d) for low energy proton beams, and additionally Mn-54 (312 d), Co-56 (77 d) and Co-60 (5.3 y) for high energy beams (intracranial collimators). Other nuclides identified with non-negligible activities were Bi-205, Bi-206 and Ga-67, but present shorter half-lives (<15 d). Mean experimental specific activities in clinical collimators one month after the irradiation are about 1000 Bq/kg (about 500 Bq/kg for low energy modulated beams) and 160 Bq/kg for ocular and intracranial collimators, respectively, for typical clinical proton doses. Differences in beam energy distribution and number of protons delivered mainly explain the variability from one collimator to another. The lower specific activities in intracranial

collimators are due to the significantly lower delivered doses (up to 4 Gy versus 52-55 Gy for ocular collimators). Otherwise, at equal doses, specific activities would be larger for intracranial collimators due to higher energies involved. Similarly, the activation on collimators irradiated with a single pristine BP is, for the same dose at the peak and same range, significantly lower than that of an SOBP, about 200 Bq/kg, because there is no contribution of the lower energy peaks. Data were not found in the literature for comparison of our results for low-energy proton beams. For high-energy proton therapy the list of isotopes from activation on brass collimators yielded in this work is fully consistent with others [3,7]. Comparison of quantitative results could only be done for one study [3] and is discussed later.

Good agreement between FLUKA and spectrometry analysis was found for non-degraded monoenergetic beams. In these cases FLUKA simulations reproduced experimental specific activities within 3% for Co-58 and Zn-65 and with a factor of 1.3 for Co-57. Except for Zn-65, differences were similar to those reported by Cesana et al [8] (monoenergetic beam of 200 MeV on a bronze collimator). The factor of 3 found by the authors for Zn-65 was attributed to the lack of cross section data in the low energy neutron library (<20 MeV) for zinc in the FLUKA version then used (2008.3.7). This explanation is compatible with the improved result obtained in this work, given that data are already available for zinc in the 2011 version here employed (JENDL 4.0 data library). Excluding Co-57, Bi-205 and Bi-206, differences lie within the 30% reported by Brugger *et al.* in the FLUKA benchmark studies on specific activities [13]. However in this and other similar FLUKA studies [20,24] comparisons were made for high energy (600 MeV-400 GeV) proton or multi-particle beams (including protons), and for materials other than brass, irradiated not in the primary but in the secondary field. At lower energies similar studies [25,36] (11 MeV and 13 MeV) show good agreement with experimental data, although results are neither directly comparable with this work. Some of the sources of experimental uncertainties might explain the higher differences obtained for Co-57, Bi-205 and Bi-206. Differences for Co-57 are not systematic and could be due to the efficiency curve, which varies drastically in this energy range and whose maximum value lies on the range of Co-57 peak. In addition, the prediction of Co-57 activity from nickel and iron is also subjected to the knowledge of the fractions of these elements in the brass alloy used. In the same line, the amounts of lead for different types of brass alloys may have very large variations (up to 80% with respect to the mean weight fraction of 2.5%). Therefore small deviations in the weight fraction of lead considered in FLUKA with respect to real fractions may have a noticeable effect on Bi-205 and Bi-206 activities. On the other hand we did not find significant differences between collimators due to the presence of the aperture: collimators N_SOBP1 (without aperture) and N_SOBP2 (with aperture), irradiated with similar SOBPs, yielded consistent activities and similar ratios between experimental and calculated activities. Therefore, the presence of the aperture, taken into account through the irradiated mass, has no perceptible effects as regards the radiation coming from the internal face of the aperture.

The complexity of FLUKA activity predictions was found to be significantly higher for modulated beams. Inaccuracies in FLUKA cross sections at different energies and for different reactions will thus have a cumulative effect for modulated beams because of the wider energy ranges involved. For clinical beams, FLUKA activities fell indeed beyond differences reported in benchmark studies (±30%). More particularly experimental activities were systematically underestimated, especially for Zn-65, but also for Co-57 and Co-58 (ratios of 2 - 5 for Zn-65, 1 – 3.6 for Co-57 and about 2 for Co-58), and more in the case of ICPO than that of CAL collimators (Table 4). The most impacted result found for Zn-65 is very likely due to the low energy yield of the reaction $^{65}Cu(p,n)^{65}Zn$. We could not find other studies in the literature showing comparisons of FLUKA activities with experimental measurements for modulated beams in proton therapy. The unrealistic proton spectral fluence considered in our model, due to the simplification of the geometry and the use of perfect monochromatic sources, was found to explain the differences for modulated beams. This issue has no impact for non-degraded single BPs with intrinsically narrow proton spectral width. The effect of the degrader on the proton spectral width has been shown elsewhere [35]. Depending on the cross sections of the different activation processes involved, the energy spread should impact to a consequent extent. Further, depth dose distributions of modulated beams composed of large energy spread beams typically present, for the same dose at the plateau, higher entrance dose at the proximal region and wider distal fall-off dose with respect to those composed by narrow energy spread beams [37]. Whereas the shape of the distal edge has no significant impact on the activation, the entrance dose does. The differences will be larger for beams with shallower penetration [37]. This fact also explains that experimental activities are underestimated by FLUKA predictions for SOBPs, and is also consistent with the larger underestimations found for fully modulated and shallower beams (e.g. N_SOBP3). Thus, an SOBP generated with multiple degraded beams will produce larger activity for each individual peak, but the dose at the entrance will in addition be larger. In this sense the higher activities obtained in ICPO collimators with respect to equivalent SOBPs in CAL collimators are also likely due to the fact that ICPO modulated depth dose distribution presents higher entrance dose and wider distal fall-off dose compared to that of CAL, typically corresponding to a larger energy spread beam. The initial energy in ICPO ocular beam line is indeed 230 MeV (from 2010), degraded down to 77 MeV with a graphite block, and further modulated in the optical bench to obtain the clinical beam.

The contribution of secondary neutrons produced along the beam line on the collimator activation was also studied. It was shown that the thermal contribution of the spectrum was ignored with the simplified geometrical model. However, for the CAL beam line the fraction of the thermal peak in the position of the collimator was found to be very low, and the activity of Zn-65 produced by the low energy neutron component negligible (<1%). The neutron component can thus be ignored in this type of calculations as long as the secondary neutron flux on the collimator is low. In this sense the larger activities of ICPO collimators with respect to those of CAL could be partially due to the higher neutron production of the first line. The ICPO ocular beam line contains indeed a second scatterer, made of lead, inside the treatment room, located less than 1.5 m upstream of the collimator. In the CAL beam line the single scatterer is located in the upstream room, separated from the treatment room by a wall of 1.9 m barite-enriched concrete, placed more than 8 m upstream of the final patient collimator. In addition the ICPO ocular beam line holds a concrete shield (about 20 cm thick) downstream of the scatterer, and a brass shield upstream of the telescopic nozzle. These two shieldings reduce the contribution of high-energy neutrons on the patient but increase at the same time that of low-energy. Further, ICPO collimators are stored for about 6 month in the treatment room before being moved to the disposal room. These factors probably increase the contribution of thermal neutrons to ICPO collimators with respect to those of CAL. Neutron activation could be particularly important in the

production of Zn-65 from zinc, since the cross-section of the neutron capture reaction $^{64}Zn(n,\gamma)^{65}Zn$ is inversely proportional to the energy in the range of thermal and low energies, with high values at thermal energies (about 40 b) and at resonance energies (cross-section peak of 60 b) [38]. In contrast, the main nuclear reactions in the production of Zn-65 by proton activation on brass, $^{65}Cu(p,n)^{65}Zn$ and $^{66}Zn(p,d)^{65}Zn$, have both maximum cross-sections lower than 1 b [39]. This reaction could thus have impacted to some extent on the results of ICPO ocular collimators. Co-60 and Cu-67 might also be produced by low energy neutrons with high cross sections at low energies. Neutron activation may thus increase the production of these isotopes if the collimators are exposed, for some reason, to an important thermal neutron flux.

The semi-empirical model presented in section 3.3 enables the determination of the residual activity in brass collimators for any proton beam, from the values of the dose, modulation, maximum beam energy and cooling time. Note that the method proposed is valid for the list of isotopes given, for energies above those indicated in Table 6, for a cooling time from 1 month to 5 years and for brass, and that the specific activity A_m is referred to the irradiated mass, as defined in this paper. An advantage of the formulation is that the modulation, as expressed in the formula (M/R), is independent of the media. Maximum and minimum activations can also be calculated with the linear and polynomial fits associated to the model (Eqs. 9 and 11) from the maximum beam energy and the dose. The model allows quantification of the influence of the different clinical parameters. In particular, a non-negligible effect of the modulation is shown, with activities rising by a factor of about 2.3 to 3.3 for full modulations as compared with monoenergetic beams. The increase in A_m/D with modulation is due to the larger number of protons required for modulated beams, for an equal dose delivered at the plateau or peak. The model could only be tested on the value of 23.4 Bq/cm^3 published by Moskvin [3] for a brass aperture irradiated with a non-modulated beam of 54 Gy at 200 MeV after 40 days cooling time, which corresponds to 3790 Bq/kg considering the irradiated mass as defined in this work. The activity yielded by the semi-empirical model for the same irradiation parameters is 804 Bq/kg. Since Moskvin's value was calculated with FLUKA, no correction should be applied and the value predicted by the model is not consistent with the author's findings. However, Moskvin's FLUKA results were not contrasted against experimental measurements.

The simplifications considered in the semi-empirical model entail an underestimation of the predicted activities related to the proton spectral fluence due to the modulation, degradation and intrinsic spectral width of the beam line. It has been shown that even for equal irradiation parameters, induced activities might differ for different beam lines. The precise quantification is therefore only possible by analyzing collimators, or by simulating with MC the beam line upstream of the collimator or entering, if known, the beam line's own proton spectral fluence. The semi-empirical model provides baseline values for ideal perfect monochromatic beams, and correction factors were proposed related to the modulation, degradation and beam line type. From the semi-empirical model, general activation levels were estimated for a typical ocular proton therapy treatment (60 MeV, total dose of 55 Gy) and for high energy treatments (100 - 220 MeV, 60 Gy). The total activity in the collimator one month after the treatment would range from 250 (non-modulated) to 800 Bq/kg (fully modulated) for ocular proton therapy and from 400 to 3000 Bq/kg for high energy proton therapy. The semi-empirical model with its associated corrections offers a practical and fast alternative to spectrometry measurements and MC calculations, to predict brass collimator activation in proton therapy centers. Although the method is only valid for brass, the behavior should be similar for other materials and the formula could thus be implemented, following the same methodology, for other media. Its extension to different proton irradiation applications other than therapy, such as isotope production, is equally conceivable. If developed for a range of typical beam line materials this approach could also be applied to dismantling processes.

6. Conclusions

The residual activity in patient brass collimators used in proton therapy one month after the treatment is of the order of 1000 and 200 Bq/kg for clinical modulated low and high energy beams, for mean delivered doses of 53 and 3.7 Gy, respectively, corresponding in turn to 19 and 54 Bq/kg·Gy. The relevant isotopes at 1 month post-irradiation are Co-57, Co-58 and Zn-65 for low energy beams and, additionally and to a lesser extent Mn-54, Co-56 and Co-60 for high energy beams. These results were derived from three independent studies carried out at the two proton therapy centers in France, which included different spectrometers, methodologies, beam lines, irradiations and collimators. Clinical and non-clinical irradiations were considered. For non-degraded monoenergetic beams FLUKA results were in agreement with experimental data and differences were globally consistent with data available in the literature. For modulated beams systematic underestimations were found, lying beyond differences reported in benchmark studies (up to a factor of 5 for Zn-65, and 2.7 for total activation). This work highlighted the significantly higher complexity of the prediction of activation for clinical (modulated) beams. Discrepancies for modulated beams were mainly attributed to the use of a simplified model considering a beam without energy spread. The impact is larger for modulated and shallower beams, and at high degradations. Differences were also found in experimental activities for different beam lines, due to variations in depth dose distributions coming from proton width spectrum characteristics. Simplified MC models provide sufficiently accurate results for monoenergetic and non-degraded beams; otherwise knowledge of proton spectrum is required to obtain precise predictions. Neutrons generated outside the collimator were proven to have a negligible impact with respect to the contribution of proton activation during a single irradiation or treatment; although it should be considered it collimators are exposed either to a high thermal neutron flux or during long time. A semi-empirical model is presented based on FLUKA simulations which yields the individual isotope activities and the total activity from proton irradiation in brass, for any SOBP of a given dose, modulation and range, and for any cooling time longer than 1 month. The use of a correction factor to take into account the proton spectral width was proposed related to the modulation, degradation and beam line type. This method represents a useful tool to easily estimate isotopes and activities for any clinical irradiation, without need of more time consuming, complex and case study methodologies. The model might be extended to other materials and to other fields and larger applications (e.g. isotope production, dismantling processes).

Acknowledgements

The authors would like to thank the ICN and the IPN for their contributions in spectrometric measurements, and in particular H. Michel, for his assistance on gamma spectrometry, as well as the staff at ICPO and CAL for their help on the practical work.

Funding

This research did not receive any specific grant from funding agencies in the public, commercial, or not-for-profit sectors.

References

[1] W.P. Levin, H. Kooy, J.S. Loeffler, T.F. DeLaney. Proton beam therapy. Br. J. Cancer, 93(8): 849-854 (2005)

[2] H. Paganetti, T. Schmitz. The influence of the beam modulation technique on dose and RBE in proton radiation therapy. Phys. Med. Biol. 41(9): 1649-1663 (1996)

[3] V. Moskvin, C. Cheng, I.J. Das. Pitfalls of tungsten multileaf collimator in proton beam therapy. Med. Phys., 38: 6395-6406 (2011)

[4] B. Gustafsson. Optimization of material in proton-therapy collimators with respect to neutron production. Examensarbete 30 hp, UPTEC ES08 030, January 2009

[5] V. Talanov, D. Kiselev, M. Wohlmuther. Numerical estimation of the equivalent dose rate after the irradiation of a tungsten collimator by a low energy proton beam. Ref. MOPRI114, proceedings of IPAC2014, Dresden, Germany, 2014

[6] H. Chen, W. Matysiak, S. Flampouri, R. Slopsema, Z. Li. Dosimetric evaluation of hybrid brass/stainless steel apertures for proton therapy. Phys. Med. Biol. 59, 5043–5060 (2014)

[7] M. Fabbender, Y.N. Shubin, V.P. Lunev, S.M. Qaim. Experimental studies and nuclear model calculations on the formation of radioactive products in interactions of medium energy protons with copper, zinc and brass: estimation of collimator activation in proton therapy facilities. Appl. Radiat. Isot., 48 (9): 1221-1230 (1997)

[8] A. Cesana, E. Mauro, M. Silari. Induced radioactivity in a patient-specific collimator used in proton therapy. Nucl. Instrum. Methods Phys. Res. B, 268: 2272–2280 (2010)

[9] C. Bungau, A. Bungau, R. Cywinski, R. Barlow, T.R. Edgecock. Induced activation in accelerator components. Phys. Rev. ST Accel. Beams, 17, 084701 (2014)

[10] B. Thomadsen, R. Nath, F.B. Bateman, J. Farr, C. Glisson, M.K. Islam, T. LaFrance, M.E. Moore, X.G. Xu, M. Yudelev. Potential hazards due to induced radioactivity secondary to radiotherapy: the report of task group 136 of the American Association of Physicists in Medicine. Health Phys., 107(5): 442-460 (2014)

[11] P.K. Walker, A.C. Edwards, I.J. Das, P.A.S. Johnstone. Radiation safety considerations in proton aperture disposal. Health Phys., 106(4): 523-527 (2014)

[12] M. Brugger, H. Khater, S. Mayer, A. Prinz, S. Roesler, L. Ulrici, H. Vincke. Benchmark studies of induced radioactivity produced in LCH materials, part II: remanent dose rates. SLAC-PUB-11812. Contributed to ICRS 10 / RPS 2004: 21st Century Challenges in Radiation Protection and Shielding, Madeira, Portugal (2004)

[13] M. Brugger, H. Khater, S. Mayer, A. Prinz, S. Roesler, L. Ulrici, H. Vincke. Benchmark studies of induced radioactivity produced in LCH materials, part I: specific activities. Radiat. Prot. Dosimetry, 116 (1–4): 6–11 (2005)

[14] M. Brugger, S. Roesler. Remanent dose rates around the collimators of the LHC beam cleaning insertions. Radiat. Prot. Dosimetry, 115 (1–4): 470–474 (2005)

[15] M.L. Sentís, A. Ferrari, S. Roesler. Calculation of the dose equivalent rate from induced radioactivity around the CNGS target and magnetic horn. CERN-OPEN-2006-016. EDMS Document No. 599104 (2005)

[16] M. Brugger, D. Forkel-Wirth, S. Roesler, J.Vollaire. Studies of induced radioactivity and residual dose rates around beam absorbers of different materials. Proceedings of HB2010, 448-452 (2010)

[17] G. Battistonni et al. The application of the Monte Carlo code FLUKA in radiation protection studies for the large hadron collider. Progress in Nuclear Science and Technology, 2: 358-364 (2011)

[18] W. Tao, Z. Kaizhi, L. Qing, L. Jidong, H. Xiaozhong, J. Xiaobing. Monte Carlo study of induced radioactivity in probe for low-energy proton beam. Nucl. Instrum. Methods Phys. Res. B, 269: 1512–1517 (2011)

[19] H. Vincke, C. Theis, S. Roesler. Induced radioactivity in and around high-energy particle accelerators. Radiat. Prot. Dosimetry, 146 (4): 434–439 (2011)

[20] P. Carbonez, F.P. La Torre, R. Michaud, M. Silari. Residual radioactivity at the CERN 600 MeV synchro-cyclotron. Nucl. Instrum. Methods Phys. Res. A, 694: 234–245 (2012)

[21] J. Blaha, F.P. La Torre, M. Silari, J. Vollaire. Long-term residual radioactivity in an intermediate-energy proton linac. Nucl. Instrum. Methods Phys. Res. A, 753:61–71 (2014)

[22] M. Brugger, A. Errahhaoui, M. Kim, H. Lee, S. Roesler, H. Vincke. Activation benchmark study at a 2.5 GeV electron

accelerator. Progress in Nuclear Science and Technology, 4: 363-366 (2014)

[23] H. Lijuan, L. Yuxiong, L. Weimin, C. Zhi, C. Yukai, R. Guangyi. Induced radioactivity analysis for the NSRL Linac in China using Monte Carlo simulations and gamma-spectroscopy. arXiv:1409.1645v1 [physics.acc-ph] (2014)

[24] F.P. La Torre, M. Silari. Leaching of radionuclides from activated soil into groundwater. J. Environ. Radioact., 143: 7-13 (2015)

[25] A. Infantino, E. Oehlke, D. Mostacci, P. Schaffer, M. Trinczek, C. Hoehr. Assessment of the production of medical isotopes using the Monte Carlo code FLUKA: Simulations against experimental measurements. Nucl. Instrum. Methods Phys. Res. B, 366:117-123 (2016)

[26] A. Carnicer, V. Letellier, G. Rucka, G. Angellier, W. Sauerwein, J. Hérault. Study of the secondary neutral radiation in proton therapy: Toward an indirect *in vivo* dosimetry. Med. Phys., 39(12): 7303-7316 (2012)

[27] J.F. Ziegler, M.D. Ziegler, J.P. Biersack. SRIM – The stopping and range of ions in matter (2010). Nucl. Instrum. Methods Phys. Res. B, 268 (11-12): 1818-1823 (2010)

[28] INTERNATIONAL ATOMIC ENERGY AGENCY, Reference Sheet for IAEA-385, 'Natural and artificial radionuclides in sediment from the Irish Sea'. IAEA, Vienna, 5 (2008)

[29] M.K. Pham et al. A new Certified Reference Material for radionuclides in Irish sea sediment (IAEA-385). Appl Radiat. Isot., 66: 1711– 1717 (2008)

[30] D. B. Pelowitz editor, "MCNP6 User's Manual, Version 1.0," LANL report LA-CP-13-00634 (2013)

[31] A. Ferrari, P.R. Sala, A. Fasso, J. Ranft. FLUKA: a multi-particle transport code", CERN 2005-10, INFN/TC_05/11, SLAC-R-773 (2005)

[32] T.T. Bohlen, F. Cerutti, M.P.W. Chin, A. Fasso, A. Ferrari, P.G. Ortega, A. Mairani, P.R. Sala, G. Smirnov, V. Vlachoudis. The FLUKA Code: Developments and Challenges for High Energy and Medical Applications. Nuclear Data Sheets 120, 211-214 (2014)

[33] V. Vlachoudis. FLAIR: A Powerful But User Friendly Graphical Interface For FLUKA. Proc. Int. Conf. on Mathematics, Computational Methods & Reactor Physics (M&C 2009), Saratoga Springs, New York (2009)

[34] R Core Team, R: A Language and Environment for Statistical Computing. R Foundation for Statistical Computing, Vienna, Austria (2014)

[35] A. Gerbershagen, A. Adelmann, R. Dölling, D. Meer, V. Rizzoglio, J.M. Schippers. Simulations and measurements of proton beam energy spectrum after energy degradation. IOP Conf. series: Journal of Physics: Conf. Series 874, 012108 (2017)

[36] Qiu R., Liu Y., Li W., Pan Y., Wang S., Lu Q., Li J. Measurement and validation of the cross section in the FLUKA code for the production of ^{63}Zn and ^{65}Zn in Cu targets for low-energy proton accelerators. Nucl. Sci. Tech., 25: S010202 (2014)

[37] W.C. Hsi, M.F. Moyers, D.Nichiporov, V.Anferov, M. Wolanski, C.E. Algower, J.B. Farr, A.E. Mascia, A.N. Schreuder. Energy spectrum control for modulated proton beams. Med. Phys., 36 (6): 2297-2308 (2009)

[38] IAEA-TECDOC-1285. Reference neutron activation library. IAEA, VIENNA (2002)

[39] N. Soppera, E. Dupont and M. Bossant. JANIS Book of proton-induced cross-sections. Comparison of evaluated and experimental data from ENDF/B-VII.1, JENDL/HE-2007, PADF-2007, TENDL-2011 and EXFOR. OECD NEA Data Bank (2012)